RESEARCH ARTICLE

Construction of the Adjusted Scoliosis 3D Finite Element Model and Biomechanical Analysis under Gravity

Jiahao Li, MM[1], Zhicheng An, MS[2], Jigong Wu, MD[3], Yongchang Gao, PhD[2] , Sheng Lu, MD[4], Da He, MD[5], Yu Zhao, MD[1]

[1]Department of Orthopaedic Surgery, Peking Union Medical College Hospital, Chinese Academy of Medical Sciences and Peking Union Medical College, [3]Chinese People's Liberation Army Strategic Support Force Characteristic Medical Center and [5]Department of Spine Surgery, Beijing Jishuitan Hospital, Beijing, [2]National Engineering Laboratory for Highway Maintenance Equipment, Chang'an University, Xi'an and [4]Department of Orthopedic Surgery, the First People's Hospital of Yunnan Province, the Affiliated Hospital of Kunming University of Science and Technology, the Key Laboratory of Digital Orthopaedics of Yunnan Provincial, Kunming, China

Objective: Adolescent idiopathic scoliosis (AIS) is a three-dimensional structural deformity of the spine caused by the disruption of the biomechanical balance of the spine. However, the current biomechanical modeling and analysis methods of scoliosis cannot really describe the real state of the spine. This study aims to propose a high-precision biomechanical modeling and analysis method that can reflect the spinal state under gravity and provide a theoretical basis for therapeutics.

Methods: Combining CT and X-ray images of AIS patients, this study constructed an adjusted three-dimensional model and FE model of the spine corresponding to the patient's gravity position, including vertebral bodies, intervertebral discs, ribs, costal cartilage, ligaments, and facet cartilage. Then, the displacement and stress of the spine under gravity were analyzed.

Results: A model of the T1-Sacrum with 1.7 million meshes was constructed. After adding the gravity condition, the maximum displacement point was at T1 of thoracic vertebra (20.4 mm). The analysis indicates that the stress on the lower surface of the vertebral body in thoracolumbar scoliosis tended to be locally concentrated, especially on the concave side of the primary curvature's vertebral body (the maximum stress on the lower surface of T9 is 32.33 MPa) and the convex side of the compensatory curvature's vertebral body (the maximum stress on the lower surface of L5 is 41.97 MPa).

Conclusion: This study provides a high-precision modeling and analysis method for scoliosis with full consideration of gravity. The reliability of the method was verified based on patient data. This model can be used to analyze the biomechanical characteristics of patients in the treatment plan design stage.

Key words: Biomechanics; Finite element; Scoliosis; Stress; X-ray

Introduction

Adolescent idiopathic scoliosis (AIS), manifested as lateral curvature and three-dimensional axial rotation of the spine, is the most common type of spine deformity in adolescents.[1] AIS patients typically present with the deformity of the torso and the body shape, resulting in the small and weak build of the patient who is accompanied by pains in the back and waist, and even symptoms of cardiac and pulmonary dysfunctions in severe patients.[2–4] Using the Cobb angle >10° as the standard, the incidence of AIS is between 2.5% and 6.93% in China.[5,6] Among the

over 0.28 billion persons younger than 15 years of age in China, there are millions of AIS patients that require intervention.

Both genetics and hormones may play roles in the pathogenesis of AIS.[7,8] More importantly, biomechanical theories, like the Hueter–Volkmann theory, have been widely recognized and discussed in the development of AIS.[9] Mechanical factors are the most important factor in the progression of scoliosis in adolescents during rapid growth and development.[10] However, data collected from cadaver spines do not reflect true biomechanical characteristics in vivo due to cell death, water loss, and tissue decay. In contrast, the finite element (FE) method is cheaper and more efficient to simulate the biomechanical analysis of scoliosis,[11] and can get specific values of the interactions between the internal organizations.[12–14] The research results can be used for the prevention and diagnosis of adolescent idiopathic spine, as well as to assist in surgery, design, and evaluation of curative effect.[15–18] However, existing biomechanical analysis studies are modeled and calculated based on only a single image data, such as CT, X-ray, or contour scans.[19] These modeling methods cannot simultaneously ensure precision and vertebral position accuracy. The position of the vertebral bodies, especially the lumbar spine, on CT images taken in the recumbent position are significantly different from X-ray taken in the upright position under gravity. X-ray and contour scanning can represent the real spinal state under gravity, but the precision of modeling is low. How to construct FE model that takes into account both model accuracy and gravity influence is an unsolved problem in previous studies.

In this study, a 3D finite element model of scoliosis was established by using both CT scan and X-ray data from a scoliosis patient. Then biomechanical analysis was carried out under load bearing condition. The aim of this study is to (i) develop a high-precision scoliosis model that fully reflects the spinal tissue state under gravity, and (ii) verify the simulation degree of the model and use for biomechanical analysis based on the data of real patients. The former model can reflect the force characteristics and position relationship of spinal soft and hard tissues under the influence of gravity in patients' daily life, which makes up for the lack of consideration in the influence of gravity on spinal tissues in the traditional high-precision modeling based on CT data. As an application attempt of the model, the latter can verify the simulation degree of the model to the real human condition, and clarify the biomechanical characteristics of the patient's spine, which is helpful to analyze the key vertebral bodies and mechanical characteristics of the patient's scoliosis and provide a reference for the design of the correction force and the application site in the treatment process.

Materials and Methods

Data Acquisition

The data was obtained from an 18-year-old girl who weighed 40 kg. The patient had typical right thoracic and left lumbar scoliotic curvatures, with a thoracic Cobb angle of 13°, and lumbar Cobb angle of 17° (Figure 1A). Cobb angle is the angle between two lines, drawn perpendicular to the upper endplate of the uppermost vertebra involved and the lower endplate of the lowest vertebra involved (Figure 1B). The patient had no history of surgery on related parts, no congenital scoliosis, or neurogenic scoliosis, and did not undergo osteotomy. According to the AIS diagnostic criteria (the Cobb angle of the coronal plane is greater than 10°), the patient was diagnosed as AIS. Conventional CT scans, using a GE Discovery CT750 HD scanner, were done on the thoracic and lumbar segment from T1 to S1 in 0.625-mm slices, yielding two-dimensional CT images of the spinal column.
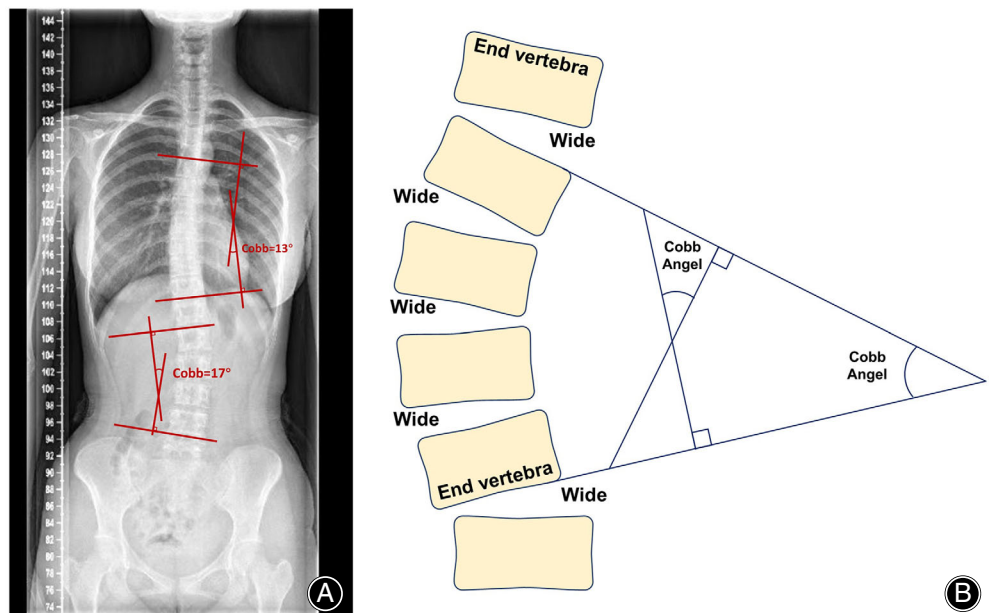

FIG. 1 X-ray image of the patient. The figure shows the patient's Cobb angle number (A) and how to measure the Cobb angle (B)

All CT images were saved in DICOM format. This study was completed with the knowledge of the subject and was supported by the Institutional Ethics Committee of Peking Union Medical College Hospital (JS-3106).

Building of the Three-Dimensional Solid Model

First, CT images of the patient were imported into Mimics 20.0 (Materialize, Leuven, Belgium), and bone tissue was extracted. After that, the target vertebrae, ribs, and other skeletal muscle structures were segmented, and the interior of the lumbar vertebrae was filled to form a mask of vertebrae. Then, the vertebrae and the rib mask were reconstructed with 3D calculation. Erase and draw features of edit masks were used to map the disc layer by layer. Then, Boolean operations were used to subtract adjacent cone masks from the disc mask and reconstruct the disc mask with 3D calculation. Finally, the CAD surface models of vertebrae, ribs, and disc were obtained. The uneven surfaces were processed using Geomagic Studio 2013(Geomagic, Inc., Research Triangle Park, NC, USA). Each surface component was then imported into Solidworks 2019 (SolidWorks Corporation, MA, USA) individually to form solid parts. The costal cartilage was established in Soliodworks 2019 according to the anatomical characteristics of the thoracolumbar spine.

The method of vertebral position adjustment based on X-ray is as follows. Take the adjustment process of T11-T12 vertebral body position as an example. First, the four corners of the vertebral body were wired to form the four outer edges of T11-L5 vertebral body on the anteroposterior spinal X-ray film. Then connect the midpoints of two pairs of edges and define the intersection point as the center point of the vertebral body. The relative positions of each two adjacent vertebrae were calculated based on the coordinates of the center point of the vertebrae (Figure 2). Finally, in SolidWorks, the T12 vertebral body is moved according to the relative position of T11 and T12, and the rotation angle on the coronal plane is adjusted in order to ensure the position of the T11-T12 articular does not interfere. Repeat the steps from T12 to L4. The position of T12-L4 was mainly adjusted in the coronal plane to ensure that there was no interference between L4 and L5 at the position of the posterior facet, and the relative position between L5 and S remained unchanged.

The facet cartilage was modeled after the spinal model was adjusted. A reference surface was made at the facet cartilage, and the external contour of the structure was drawn by spline curve. The surface-surface contact elements were used to simulate facet joints Then, the generating plane and thickening command were used, and the overlap part with the adjacent two cones was deleted by combination command (Figure 3).

The Establishment of Finite Element Model

Bone tissue was regarded as a uniform, isotropic, and coherent linear elastic material. Intervertebral disc annulus fibrosus were set as isotropic, uniform, and continuous elastomer, referring to previous research data.[20] Intervertebral discs were not divided into annulus fibrosus and nucleus pulposus. Intervertebral disc materials used annulus fibrosus material values, and material properties are shown in Table 1
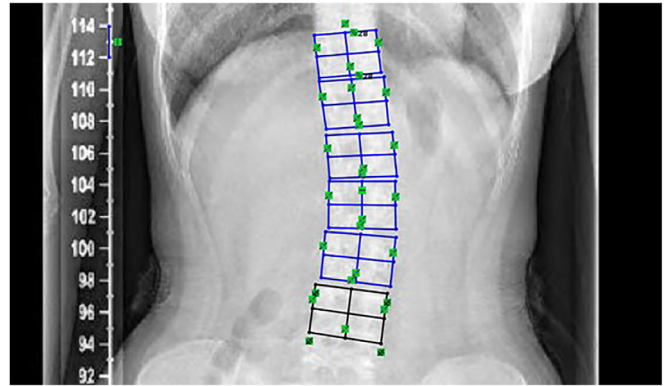

FIG. 2 Determination of the center of the vertebral body. The lines in the figure are the line between the edges and midpoints of the vertebral body. The central point of the vertebral body is determined by the midpoint connection

below. In Abaqus 2018 (Dassault, Providence, RI, USA), the ligament parameters were used to set the rod unit, and the stiffness value of the rod unit under each parameter was measured as the stiffness value required by the spring elements to simulate the ligament. A total of seven spring elements were constructed between each two vertebral bodies to simulate the whole model with 119 spring elements.

The intervertebral disc and vertebrae contact surfaces, costal cartilage and sternum, and vertebral body contact surfaces were restrained by binding. The articular surface of the posterior facet was set as the facet contact small slip facet cartilage. One side was set as the binding constraint, and the other side was set as the facet contact small slip. The constraint between the vertebra and the upper reference point (2.5 mm above the centroid of the endplate) was defined as the coupling constraint. To verify the sensitivity of mesh size, the mesh sizes of cortical bone and annulus fibrosus were changed to 1.5 mm, 2 mm, and 2.5 mm, respectively. A bending moment of 10 N·m was applied to the L5-S vertebral body to perform forward flexion test.

Boundary and Loading Conditions

Based on the patient's body weight of 40 kg, the loading on each vertebral body in the finite element model was calculated, and the effects of gravity factors were simulated. The formula is calculated as follows:

$$Ptot_i = (15 + 2.1 \times Mass_i)$$

$$\Delta(Ptot_i) = Ptot_i - Ptot_{i-1},$$

$$\Delta(Force_i) = \Delta(Ptot_i) \times g, g = 9.81 \, ms^{-2}$$

$$Mass_i = Weight \ of \ vertebral \ segment \ i \ (kg)$$

$$Ptot_i = Total \ weight \ above \ the \ vertebral \ segment \ i$$

Constrain all degrees of freedom on the lower surface of the sacrum. The other models did not have constraints.

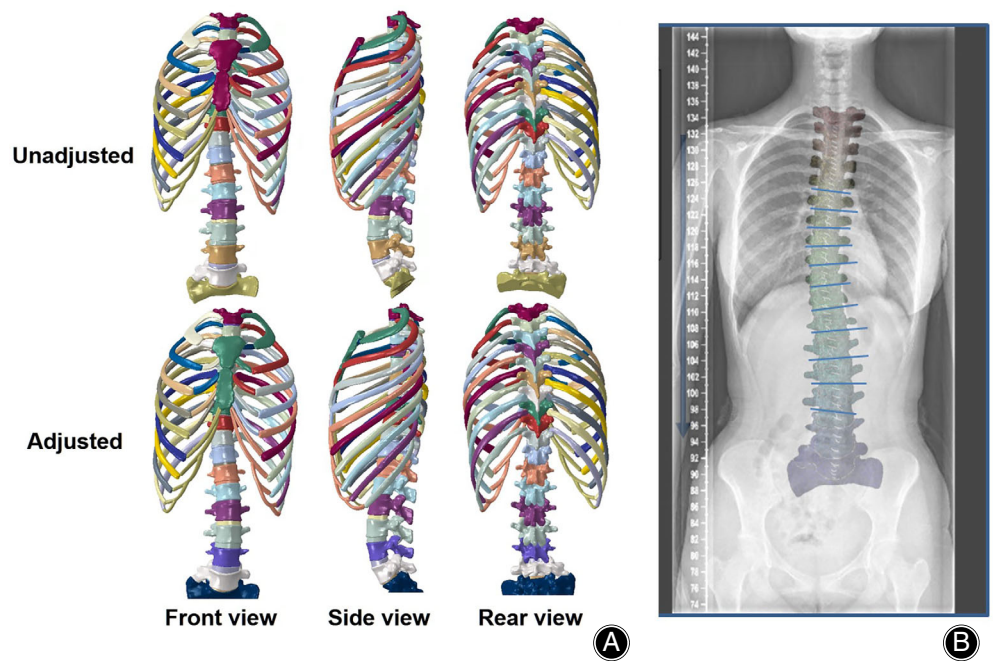SCOLIOSIS FINITE ELEMENT ANALYSIS UNDER GRAVITY

FIG. 3 3D model of scoliosis before and after adjustment according to X-ray (A) and its comparison with X-ray (B). The position of the vertebral body after adjustment is more in line with the actual situation of the patient in the gravity position

TABLE 1 Material parameters of thoracolumbar FE model			
Materials	Young's Modulus (MPa)	Poisson ratio	Stiffness (N/mm)
Cortical bone	12,000	0.3	
Cancellous bone	100	0.2	
Annulus fibrosis	4.2	0.45	
Costal cartilage	300	0.2	
Facet cartilage	1000	0.3	
Anterior longitudinal ligament			33.3
Posterior longitudinal ligament			20.4
Supraspinous ligament			23.7
Interspinous ligament			11.5
Ligamentum flavum			27.2
Intertransverse ligament			23.2

Parameter Measurement

Displacement is defined as the distance between the spatial positions of any point on the model before and after the loading condition. Angular migration represents the angle change of L4-5 transcentroid axis before and after loading conditions. Stress is the pressure value at each point on the lower surface of the vertebral body after loading conditions. The above data are output by Solidworks 2019 after loading the conditions.

Results

FE Model

The total number of T1-Sacrum meshes is 1.7 million. The number of meshes for each model is mainly determined by model shape and size and warning cells. Mesh properties are shown in Table 2 below. The FE model includes finely

Table 2 Mesh properties			
Materials	Cell type	Mesh size	Mesh quantity
Cortical bone	C3D10	1.6–1.8	28,000–40,000
Cancellous bone	C3D4	2–2.3	25,000–36,000
Intervertebral disc	C3D10	1.2	14,000–35,000
Costal cartilage	C3D4	2.2	1000–30,000
Facet cartilage	C3D10	0.4	2000–5000

reconstructed various vertebral bodies, intervertebral discs, costal cartilage, and facet cartilage.

Mesh Independence Verification

The results of the mesh independence verification are shown in Figure 5A,B. When the mesh size was 1.5 mm, 2 mm, and 2.5 mm, the displacement error between the two adjacent mesh sizes was less than 5% in the simulated L1-S vertebral
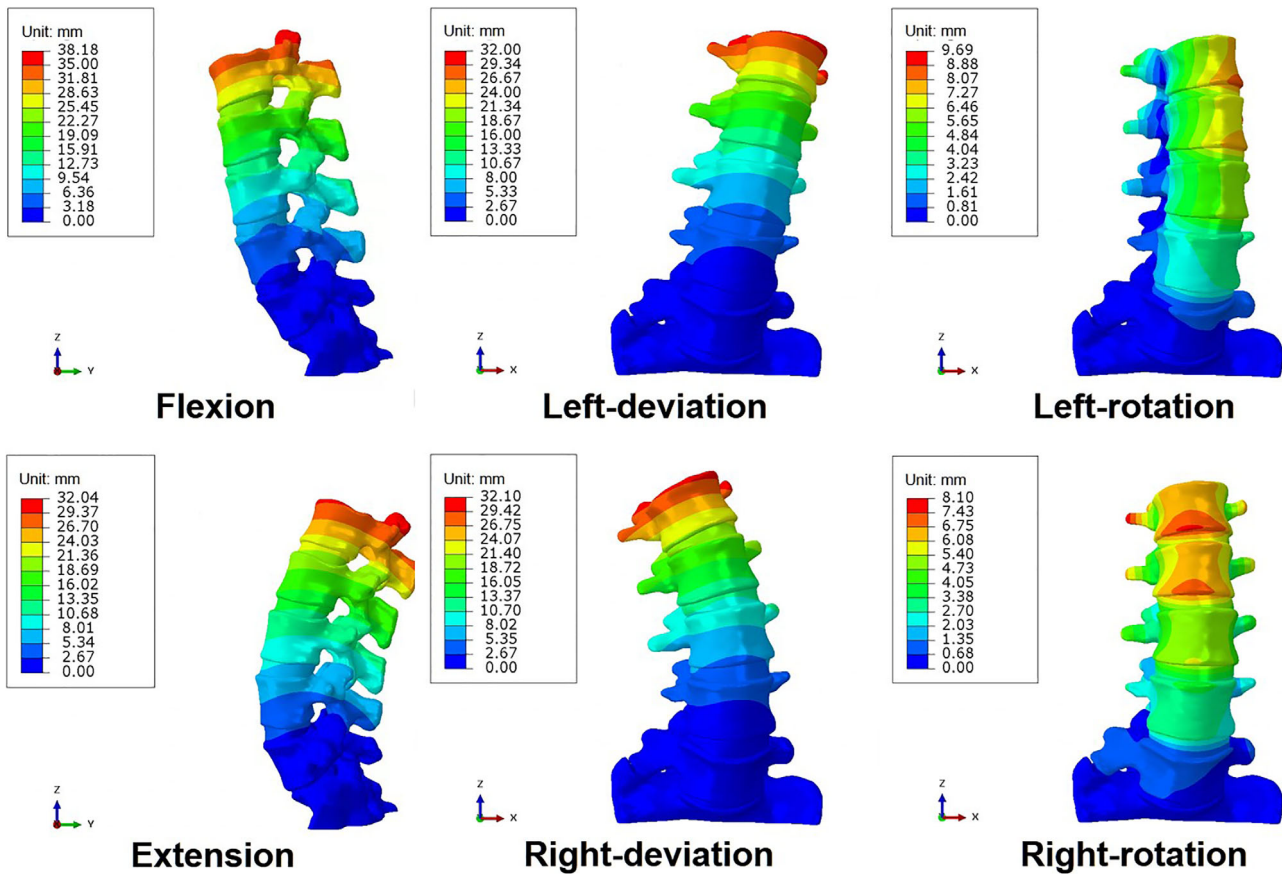
FIG. 4 Displacement field for model validation. This figure shows the displacement of lumbar vertebrae in the model under six motion states (flexion, extension, left-deviation, right-deviation, left-rotation, and right-rotation). Unit: mm

body flexion state. Under the above conditions, the stress value error on the lower surface of L5 between two adjacent mesh sizes is less than 5%. Therefore, the mesh size we have chosen is within a reasonable range.

Displacement and ROM of the Entire Lumbar Spine

The analysis of the displacement in six directions after the loading of 10 N·M force moment to lumbar vertebra L1-S is shown in Figure 4. The maximum position deviation in all six directions occurred in L1 vertebra, which is consistent with clinical practice. After the loading of 10 N·M force moment to lumbar vertebra L1-S, the angular migration obtained through the constructed 3D finite element model in flexion, extension, left-deviation, right-deviation, left-rotation, and right-rotation were 4.75°, 4.00°, 4.60°, 4.32°, 2.82°, and 3.00°, respectively. We show Yamamoto's research data[21] and our results in Figure 5C.

Displacement and Stress Distribution of each Vertebra

Equivalent displacement field and the simplified spine curve of thoracolumbar scoliosis model under simulated gravity (ribs, costal cartilage, and sternum are hidden) are shown in

Figure 6. It can be seen that after loading gravity on the scoliosis model, the vertebral body in double bends in the coronal plane moved to the curved side, aggravating the degree of scoliosis, and the thoracic vertebral body moved backward in the sagittal plane. The maximum displacement point was at T1 of thoracic vertebra (20.4 mm).

Figure 7 shows the equivalent stress field of the lower surface of each vertebral body under simulated gravity in the thoracolumbar scoliosis model. The maximum stress is located on the concave side (right side) of L5 (41.97 MPa), fitting our perception. Surprisingly, the stress in the thoracic segment was greater on the convex side (right side of T9, 32.33 MPa). Part of the maximum stress occurs in the mesh below the surface edge of the vertebrae. Stress concentration occurs where the medial curvature of cortical bone is large (the rounded corner formed on the upper and lower surfaces and lateral surfaces of the vertebrae), as shown in Figure 8.

Discussion

This study presents a novel high-precision biomechanical model and analysis method for scoliosis that combines CT and X-ray images to more accurately reflect the
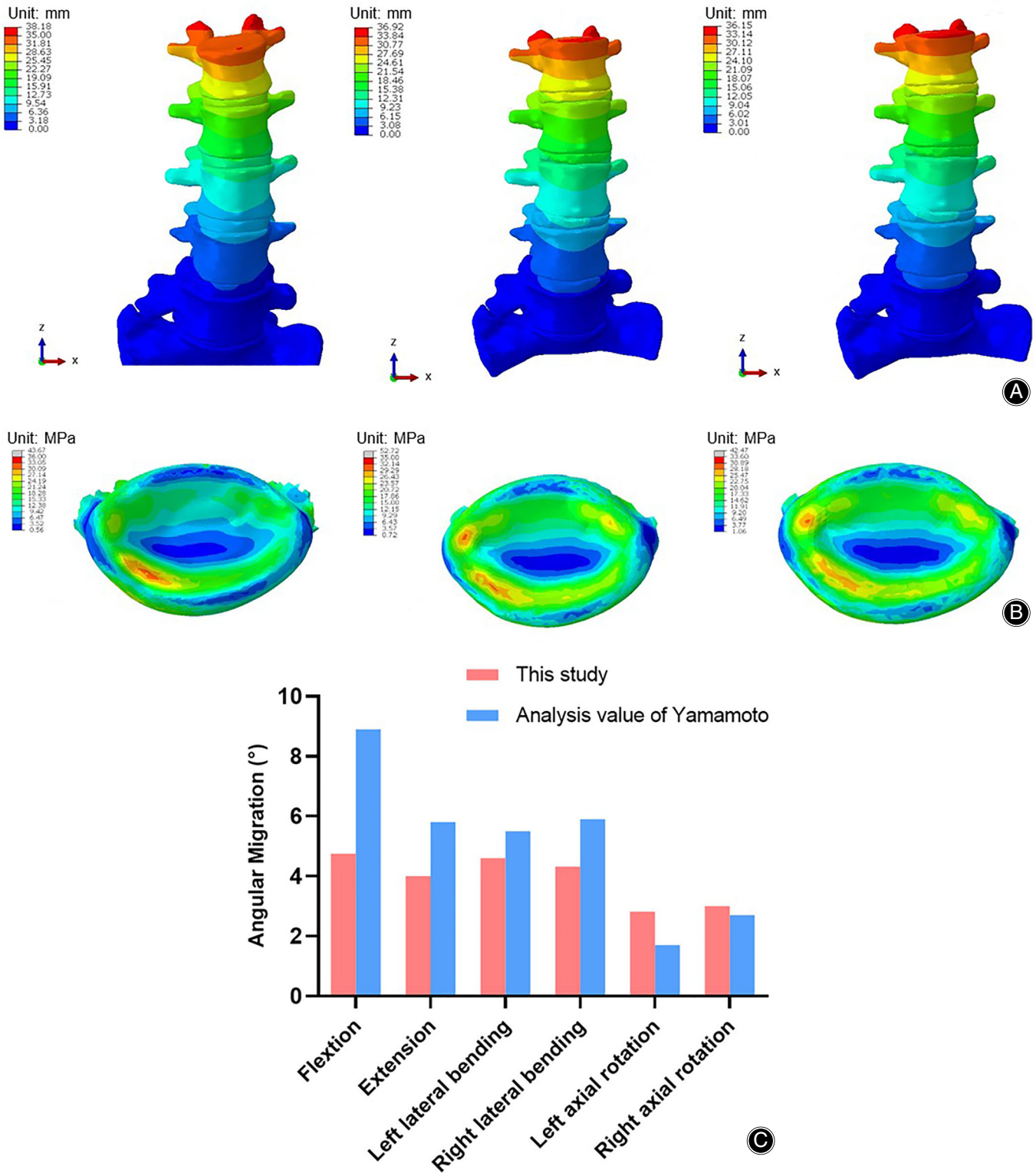
FIG. 5 Finite element model verification. (A) the L1-S vertebral displacement under forward flexion was simulated when the mesh size was 1.5 mm, 2 mm, and 2.5 mm, respectively. (B) When the mesh size was 1.5 mm, 2 mm, and 2.5 mm, the stress distribution on the lower surface of S vertebral body was simulated under forward flexion condition. (C) The angular migration of the lumbar vertebrae in the established model under six motion states (flexion, extension, left bending, right bending, left rotation, and right rotation) were compared with the literature data
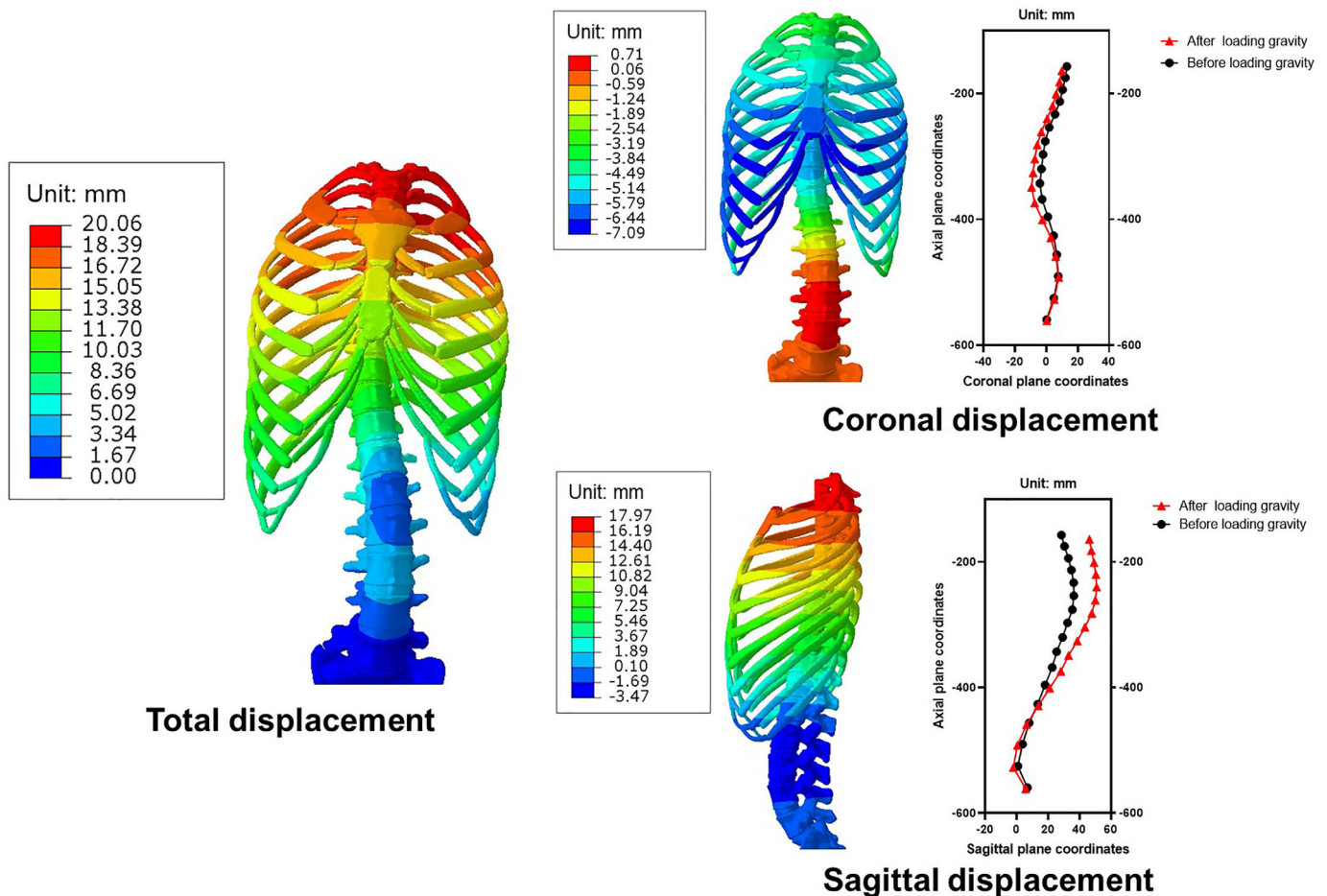
FIG. 6 Equivalent displacement field of thoracolumbar scoliosis model under simulated gravity. This figure shows the displacement of the vertebral body in different directions (general, coronal, sagittal) of the model after the application of gravity. The curve on the right of the displacement field plot shows the simplified vertebral position curve before and after gravity conditions were applied. The warmer the color, the greater the displacement. Unit: mm

biomechanical characteristics of scoliosis under gravity. The feasibility of the method was verified by the analysis of a real clinical sample data. This approach is expected to be used to guide the therapeutics of scoliosis in the future.

High-Precision Modeling under Gravity

Three-dimensional reconstruction and finite element analysis of the vertebral bodies and their surrounding tissues of scoliosis patients are important methods to study the biomechanical changes in the development of scoliosis.[22] However, the current high-precision scoliosis models are mainly based on a single image data, such as CT, X-ray, or contour scans.[23] CT images were acquired in the supine position and do not reflect the biomechanical changes in the spine under gravity during standing or sitting in daily life. X-ray is taken in a standing position, which can represent the biomechanical properties of the spine under gravity. However, the resolution of X-ray images is low, and the modeling accuracy based

on X-ray images is not as high as that based on CT images. Especially in patients with small Cobb angles, this difference can bias the results of biomechanical analysis more severely. Asymmetrical activation and asymmetrical weakness of muscles around the spine contribute to the cause of AIS,[24] especially affecting the coronal position of the vertebral body. Unlike the sagittal curve, which can form a curve close to the physiological state after applying gravity conditions on the FE model, the coronal curve is influenced by multidirectional muscle forces in standing position. Some studies have modeled muscles to simulate their impact on the spine,[25] but this method was not used in this study because of the lack of data in the current literature and the difficulty in defining the value of muscle force after scoliosis. However, only applying gravity to FE model based on CT data reconstruction is difficult to simulate the real situation. Besides, the model reconstructed only based on X-ray image is limited by less image information and low accuracy. In addition,
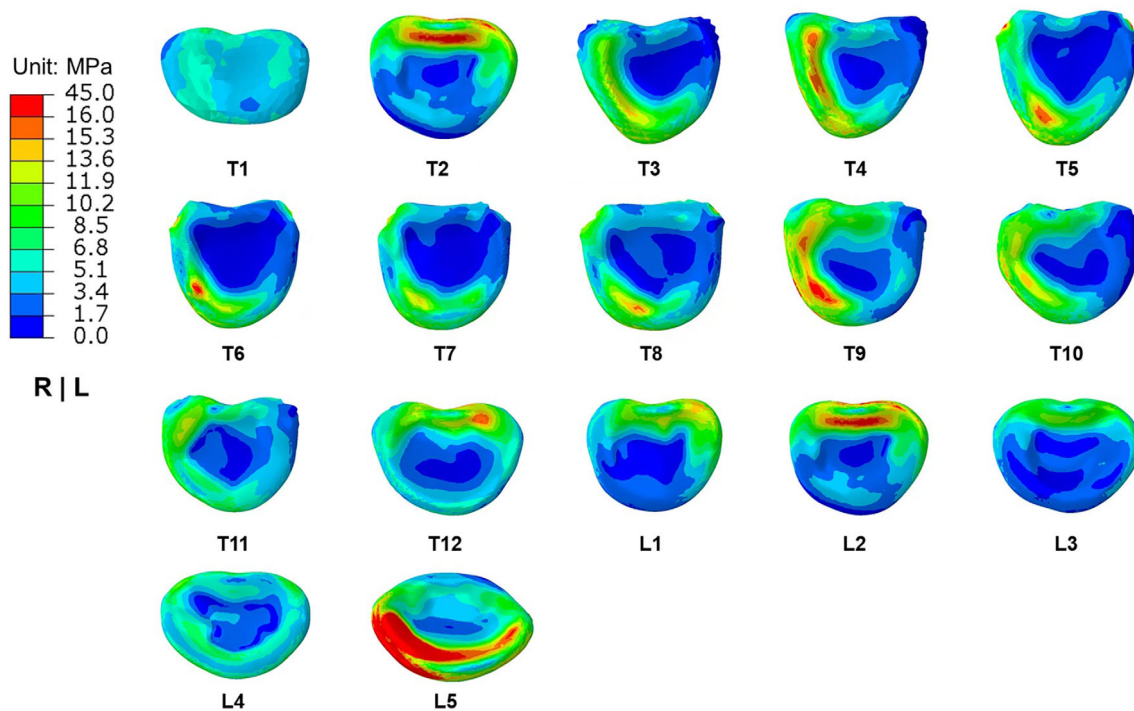
FIG. 7 Field of equivalent stress on the lower surface of each vertebral body. This diagram shows the stress distribution on the lower surface of the vertebral body, with warmer colors indicating greater stress. Unit: MPa
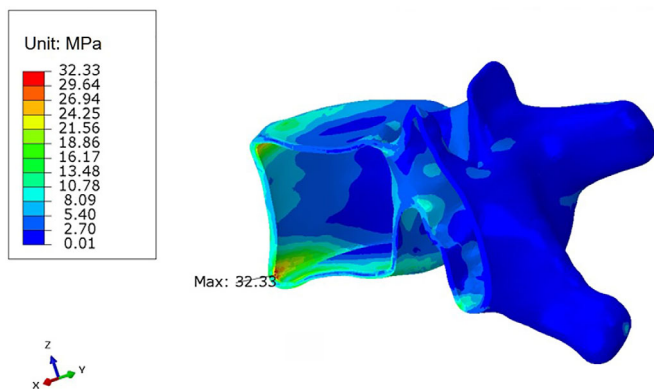

FIG. 8 Section view of T9's equivalent stress field. This figure shows the stress distribution of the T9 vertebral body, with warmer colors indicating greater stress. Unit: MPa

contour scanning cannot show deep tissue such as vertebral body, disc ligament, and so on, so the established model is not suitable for the study of the progression of scoliosis. For the above reasons, we constructed a method to adjust the displacement of the scoliosis model (especially the lumbar spine) according to the X-ray images after CT image reconstruction, to simulate the real posture of the spine of scoliosis patients in the daily gravity state. From a biomechanical point of view, this method not only helps to simulate the most realistic spinal forces, but also applies to the movement of the spine and the deflection of position after receiving external forces, such as corrective forces from braces.

Finite Element Analysis Considering the Mechanical Action of Hard and Soft Tissues

Previous finite element analysis of scoliosis usually only considered the bony structure of the spine, that is, the biomechanics of the vertebral body.[26,27] However, in recent years, more and more attention has been paid to the interaction between the vertebral column and the surrounding structures, such as intervertebral discs, articular cartilage, ligaments, muscles, and even internal organs.[22,28] Scoliosis causes pathological changes in the bone, discs, and ligaments, resulting in a narrowing of the intervertebral space on the concave side and a widening of the intervertebral space on the convex side. In addition, facet joints and spinous processes can also have a vital impact on the force of the spine. Therefore, the influence of ribs, facet joints, discs, and ligaments, especially their mechanical antagonism and position limitation, need to be considered when biomechanical analysis is performed. Hence, we used spring elements to simulate ligaments and constructed the facet cartilage, the sternum, ribs, costal cartilage, and pelvis based on CT images. Though FE method can only provide a biomechanical analysis for varieties of biological tissue as a homogeneous material, it is one of the best ways to study biomechanics in vivo. By refining models as much as

possible, it is expected to be able to maximize the biological tissues in the body to actual status and parameters. Thus, the most realistic FE analysis results can be obtained to guide the study of etiology and treatment.

The Range of Motion Difference between the Model and the Real Spine

The lumbar spine has a relatively large degree of activity in vivo. In this study, the lumbar ROM of the ais model was smaller than that of the actual lumbar spine. This may be caused by lumbar scoliosis and abnormal deformation of the lumbar spine in AIS patients. compared with the in vitro study by Yamamoto *et al.*,[21] the stiffness of FE method in flexion, extension, and lateral bending was greater than that of normal cadaver lumbar vertebrae. This phenomenon can be explained by the understanding that scoliosis causes morphological and structural changes in the lumbar spine.[29] Thus, the movement of the lumbar spine is limited. Or it may be due to the different geometry used by the material properties. The presence of fluid in the nucleus pulposus and annulus fibrosus, both in vivo and in vitro, causes the disc to be highly flexible. However, no studies have investigated the applicability of nonlinear versus linear material properties in scoliosis. While in FE analysis, solid elements are used to simulate discs, so it is difficult to simulate nonlinear characteristics, resulting in higher stiffness of the FE method intervertebral disc than that of cadaver intervertebral disc. As muscle tissue was not included in the model of this study, the limitation of muscle tissue on vertebral body activity was not considered.[30] This may result in a higher degree of rotational motion in the lumbar spine than in vitro experiment.

Biomechanics of Scoliosis under Gravity

AIS patients have asymmetrical forces. When AIS patients stood, the maximum plantar pressure on the concave side of the lower extremity was higher than that on the convex side.[31] In this study, when gravity was applied, the spine shifted to the curved side, aggravating the degree of scoliosis. According to the equivalent stress field of coronal plane and sagittal plane of the spine after loading, the concave side stress of the medial vertebral body at the bend is greater than the convex side stress in the lumbar segment. After scoliosis occurs, the stress must be asymmetrically distributed. According to Wolf's Law, the distribution of stress affects bone growth to adapt to a complex external environment. The growth of each part of the spine is related to the stress it is subjected to. The Hueter–Volkmann principle[32] illustrates that when the spine is in a stress concentration position, the growth of bone is inhibited, resulting in skeletal hypoplasia. And bone growth restores when the stress is disappeared. Scoliosis can occur with changes in loaded bone.[33] While the asymmetry of pedicle geometry or growth rate was an independent cause of scoliosis.[34] The patient in this study had double curvature, with a greater degree of lumbar curvature than thoracic curvature. We observed an unexpected concentration of stress on the convex side of the thoracic curvature on the stress field. This may be interpreted as the lumbar curvature is the primary curvature, and the thoracic curvature is the body's compensation curvature to maintain the force line. As the right side of the primary lumbar curvature is concave, the growth of the right side of the vertebral body in the compensatory thoracic curvature is accelerated to form a convex side. The stress concentration on the convex side of thoracic curvature may be caused by asymmetrical growth of the lower surface of the vertebral body. In addition, asymmetric growth of the spine will result in scoliosis and axial rotation in the deformity of scoliosis.[35] Patients in this study had low Cobb Angle numbers and no significant trunk rotation was observed. However, the etiology and progression of AIS are multifaceted and cannot be explained only by the imbalance of stress on the spine. Whether asymmetric loads on the vertebrae and discs are the cause of AIS remains controversial.[36,37]

Strengths and Limitations

There are some limitations in this study: the validity of the FE model is determined by comparing the data with the experimental model. Usually, a suitable experimental model is retrieved from the literature. If the FE calculation results are in good agreement with the experimental results, this indicates that the model is effective. However, experimental models do not necessarily reflect what's going on inside the body. Although the FE model can explain the experimental results well, its independent prediction ability is limited. In addition, the FE model has many simplifications and assumptions, and the simulation of biological tissue does not completely conform to the real situation. Some studies have modeled the annulus fibrosus and nucleus pulposus of intervertebral discs separately,[38] but this study has not divided them. In this study, CT data used in the FE model were obtained from a case of AIS. Due to the limited number of samples, the influence of bending type on measurement results cannot be excluded. The biomechanical role of soft tissue and muscle was not fully considered in this study due to the immaturity of current muscle modeling methods. However, this study will help us understand the stress and displacement characteristics of adolescent idiopathic scoliosis patients and further understand the progression changes and offer potential value in the treatment of AIS.

Conclusions

A finite element model of a patient with bicurved scoliosis was established, based on CT images and adjusted for lumbar spatial position using X-rays. The analysis indicates that the stress on the lower surface of the vertebral body in thoracolumbar scoliosis tended to be locally concentrated, especially on the concave side of the primary curvature's vertebral body and the convex side of the compensatory curvature's vertebral body. It provides a new concept and biomechanical method for the study of progression and treatment of scoliosis.

Authors' Contributions

J.H.L. and Z.C.A. contribute equally to this work. Y.Z., Y.C.G., and D.H. conceived, designed, and supervised the study; J.H.L., Z.C.A., J.G.W. and S.L. conduct experiments and led the statistical analysis of the data. The first draft of the manuscript was written by J.H.L. All authors read and approved the final manuscript before submission.

Authorship Declaration

All authors listed meet the authorship criteria according to the latest guidelines of the International Committee of Medical Journal Editors. All authors are in agreement with the manuscript.

Ethical Statement

This study was completed with the knowledge of the subject and was supported by the Institutional Ethics Committee of Peking Union Medical College Hospital (JS-3106).

Conflict of Interest

All authors declare that they have no financial and personal relationships with other people or organizations that can inappropriately influence our work, there is no professional or other personal interest of any nature or kind in any product, service, and/or company that could be construed as influencing the position presented in, or the review of, the manuscript.

References

1. Reamy BV, Slakey JB. Adolescent idiopathic scoliosis: review and current concepts. Am Fam Physician. 2001;64(1):111–6.
2. Altaf F, Gibson A, Dannawi Z, Noordeen H. Adolescent idiopathic scoliosis. BMJ. 2013;346:f2508. https://doi.org/10.1136/bmj.f2508
3. Burton MS. Diagnosis and treatment of adolescent idiopathic scoliosis. Pediatr Ann. 2013;42(11):224–8. https://doi.org/10.3928/00904481-20131022-09
4. Kim W, Porrino JA, Hood KA, Chadaz TS, Klauser AS, Taljanovic MS. Clinical evaluation, imaging, and management of adolescent idiopathic and adult degenerative scoliosis. Curr Probl Diagn Radiol. 2019;48(4):402–14. https://doi.org/10.1067/j.cpradiol.2018.08.006
5. Zheng Y, Dang Y, Wu X, Yang Y, Reinhardt JD, He C, et al. Epidemiological study of adolescent idiopathic scoliosis in eastern China. J Rehabil Med. 2017;49(6):512–9. https://doi.org/10.2340/16501977-2240
6. Li C, Zhang B, Liu L, Li Y, Xu Y, Wang L, et al. Design, reliability, and validity of a portable electronic device based on ergonomics for early screening of adolescent scoliosis. J Orthop Translat. 2021;28:83–9. https://doi.org/10.1016/j.jot.2020.10.014
7. Cheng JC, Castelein RM, Chu WC, Danielsson AJ, Dobbs MB, Grivas TB, et al. Adolescent idiopathic scoliosis. Nat Rev Dis Primers. 2015;1:15030. https://doi.org/10.1038/nrdp.2015.30
8. Esposito T, Uccello R, Caliendo R, Di Martino GF, Gironi Carnevale UA, Cuomo S, et al. Estrogen receptor polymorphism, estrogen content and idiopathic scoliosis in human: a possible genetic linkage. J Steroid Biochem Mol Biol. 2009;116(1–2):56–60. https://doi.org/10.1016/j.jsbmb.2009.04.010
9. Stokes IA, Mente PL, Iatridis JC, Farnum CE, Aronsson DD. Enlargement of growth plate chondrocytes modulated by sustained mechanical loading. J Bone Joint Surg Am. 2002;84(10):1842–8. https://doi.org/10.2106/00004623-200210000-00016
10. Fadzan M, Bettany-Saltikov J. Etiological theories of adolescent idiopathic scoliosis: past and present. Open Orthop J. 2017;11:1466–89. https://doi.org/10.2174/1874325001711011466
11. Zhang Y, Gan Y, Niu W, Norrman K, Yan X, Christensen DV, et al. Tuning the two-dimensional electron gas at oxide interfaces with Ti-O configurations: evidence from X-ray photoelectron spectroscopy. ACS Appl Mater Interfaces. 2018;10(1):1434–9. https://doi.org/10.1021/acsami.7b16510
12. Kumaresan S, Yoganandan N, Pintar FA, Maiman DJ, Kuppa S. Biomechanical study of pediatric human cervical spine: a finite element approach. J Biomech Eng. 2000;122(1):60–71. https://doi.org/10.1115/1.429628
13. Belytschko T, Kulak RF, Schultz AB, Galante JO. Finite element stress analysis of an intervertebral disc. J Biomech. 1974;7(3):277–85. https://doi.org/10.1016/0021-9290(74)90019-0
14. Tran TQ, Lee HP, Lim SP. Modelling porous structures by penalty approach in the extended finite element method. Comput Methods Biomech Biomed Engin. 2013;16(4):347–57. https://doi.org/10.1080/10255842.2011.621120
15. Noda M, Saegusa Y, Takahashi M, Tezuka D, Adachi K, Naoi K. Biomechanical study using the finite element method of internal fixation in Pauwels type III vertical femoral neck fractures. Arch Trauma Res. 2015;4(3):e23167. https://doi.org/10.5812/atr.23167

16. Li J, Zhao X, Hu X, Tao C, Ji R. A theoretical analysis and finite element simulation of fixator-bone system stiffness on healing progression. J Appl Biomater Funct Mater. 2018;16(3):115–25. https://doi.org/10.1177/2280800017750357
17. Cheung JPY, Yiu KKL, Vidyadhara S, Chan PPY, Cheung PWH, Mak KC. Predictability of supine radiographs for determining in-brace correction for adolescent idiopathic scoliosis. Spine (Phila Pa 1976). 2018;43(14):971–6. https://doi.org/10.1097/BRS.0000000000002503
18. Zadpoor AA, Weinans H. Patient-specific bone modeling and analysis: the role of integration and automation in clinical adoption. J Biomech. 2015;48(5):750–60. https://doi.org/10.1016/j.jbiomech.2014.12.018
19. Lukovic V, Cukovic S, Milosevic D, Devedzic G. An ontology-based module of the information system ScolioMedIS for 3D digital diagnosis of adolescent scoliosis. Comput Methods Programs Biomed. 2019;178:247–63. https://doi.org/10.1016/j.cmpb.2019.06.027
20. Liu X, Ma J, Park P, Huang X, Xie N, Ye X. Biomechanical comparison of multilevel lateral interbody fusion with and without supplementary instrumentation: a three-dimensional finite element study. BMC Musculoskelet Disord. 2017;18(1):63. https://doi.org/10.1186/s12891-017-1387-6
21. Yamamoto I, Panjabi MM, Crisco T, Oxland T. Three-dimensional movements of the whole lumbar spine and lumbosacral joint. Spine (Phila Pa 1976). 1989;14(11):1256–60. https://doi.org/10.1097/00007632-198911000-00020
22. Guan T, Zhang Y, Anwar A, Zhang Y, Wang L. Determination of three-dimensional corrective force in adolescent idiopathic scoliosis and biomechanical finite element analysis. Front Bioeng Biotechnol. 2020;8:963. https://doi.org/10.3389/fbioe.2020.00963
23. Little JP, Adam CJ. Geometric sensitivity of patient-specific finite element models of the spine to variability in user-selected anatomical landmarks. Comput Methods Biomech Biomed Engin. 2015;18(6):676–88. https://doi.org/10.1080/10255842.2013.843673
24. Park Y, Ko JY, Jang JY, Lee S, Beom J, Ryu JS. Asymmetrical activation and asymmetrical weakness as two different mechanisms of adolescent idiopathic scoliosis. Sci Rep. 2021;11(1):17582. https://doi.org/10.1038/s41598-021-96882-8
25. Kamal Z, Rouhi G, Arjmand N, Adeeb S. A stability-based model of a growing spine with adolescent idiopathic scoliosis: a combination of musculoskeletal and finite element approaches. Med Eng Phys. 2019;64:46–55. https://doi.org/10.1016/j.medengphy.2018.12.015
26. Hadagali P, Peters JR, Balasubramanian S. Morphing the feature-based multi-blocks of normative/healthy vertebral geometries to scoliosis vertebral geometries: development of personalized finite element models. Comput Methods Biomech Biomed Engin. 2018;21(4):297–324. https://doi.org/10.1080/10255842.2018.1448391
27. Song XX, Jin LY, Li XF, Qian L, Shen HX, Liu ZD, et al. Effects of low bone mineral status on biomechanical characteristics in idiopathic scoliotic spinal deformity. World Neurosurg. 2018;110:e321–9. https://doi.org/10.1016/j.wneu.2017.10.177
28. Zhang Q, Chon T, Zhang Y, Baker JS, Gu Y. Finite element analysis of the lumbar spine in adolescent idiopathic scoliosis subjected to different loads.

SCOLIOSIS FINITE ELEMENT ANALYSIS UNDER GRAVITY

Comput Biol Med. 2021;136:104745. https://doi.org/10.1016/j.compbiomed. 2021.104745

29. Addai D, Zarkos J, Bowey AJ. Current concepts in the diagnosis and management of adolescent idiopathic scoliosis. Childs Nerv Syst. 2020;36(6): 1111–9. https://doi.org/10.1007/s00381-020-04608-4

30. Bruno AG, Mokhtarzadeh H, Allaire BT, Velie KR, De Paolis Kaluza MC, Anderson DE, et al. Incorporation of CT-based measurements of trunk anatomy into subject-specific musculoskeletal models of the spine influences vertebral loading predictions. J Orthop Res. 2017;35(10):2164–73. https://doi.org/10.1002/jor.23524

31. Chockalingam N, Bandi S, Rahmatalla A, Dangerfield PH, Ahmed el N. Assessment of the centre of pressure pattern and moments about S2 in scoliotic subjects during normal walking. Scoliosis. 2008;3:10. https://doi.org/10.1186/1748-7161-3-10

32. Stokes IA. Mechanical modulation of spinal growth and progression of adolescent scoliosis. Stud Health Technol Inform. 2008;135:75–83.

33. Goto M, Kawakami N, Azegami H, Matsuyama Y, Takeuchi K, Sasaoka R. Buckling and bone modeling as factors in the development of idiopathic scoliosis. Spine (Phila Pa 1976). 2003;28(4):364–70; discussion 371. https://doi.org/10.1097/01.BRS.0000048462.90775.DF

34. Huynh AM, Aubin CE, Rajwani T, Bagnall KM, Villemure I. Pedicle growth asymmetry as a cause of adolescent idiopathic scoliosis: a biomechanical study. Eur Spine J. 2007;16(4):523–9. https://doi.org/10.1007/s00586-006-0235-4

35. Stokes IA, Laible JP. Three-dimensional osseo-ligamentous model of the thorax representing initiation of scoliosis by asymmetric growth. J Biomech. 1990;23(6):589–95. https://doi.org/10.1016/0021-9290(90)90051-4

36. Brink RC, Homans JF, Schlosser TPC, van Stralen M, Vincken KL, Shi L, et al. CT-based study of vertebral and intravertebral rotation in right thoracic adolescent idiopathic scoliosis. Eur Spine J. 2019;28(12):3044–52. https://doi.org/10.1007/s00586-019-06138-3

37. Vavruch L, Forsberg D, Dahlstrom N, Tropp H. Vertebral axial asymmetry in adolescent idiopathic scoliosis. Spine Deform. 2018;6(2):112–20 e111. https://doi.org/10.1016/j.jspd.2017.09.001

38. Areias B, Caetano SC, Sousa LC, Parente M, Jorge RN, Sousa H, et al. Numerical simulation of lateral and transforaminal lumbar interbody fusion, two minimally invasive surgical approaches. Comput Methods Biomech Biomed Engin. 2020;23(8):408–21. https://doi.org/10.1080/10255842.2020.1734579